Coherence properties of blackbody radiation between parallel plates

1979 J. Phys. A: Math. Gen. 12 1563

(http://iopscience.iop.org/0305-4470/12/9/023)

J. Phys. A: Math. Gen., Vol. 12, No. 9, 1979. Printed in Great Britain

Coherence properties of blackbody radiation between parallel plates

W Eckhardt

Abteilung für Theoretische Physik, Universität Ulm, 7900 Ulm, West Germany

Received 30 August 1978, in final form 4 December 1978

Abstract. The coherence of blackbody radiation between two parallel (distance L apart), infinitely extended and perfectly conducting plates is studied. The finite size of the geometric arrangement leads to spatially dependent coherence properties which are compared with the spatially averaged properties.

1. Introduction

It is well known that blackbody radiation can be characterised by the degree of greatest possible incoherence compared with other radiation sources. This statement requires that the thermal radiation is not influenced by boundary conditions. Nevertheless, the infinite-space blackbody radiation reveals ranges of space and time in which the coherence is different from zero. The fundamental studies in this field were made by Bourett (1960), Sarfatt (1963) and Mehta and Wolf (1964a, b, 1967).

The standard quantity for the description of radiation fields is the complex degree of coherence. The quantity can be measured directly by interference experiments (Mandel and Wolf 1965). It is expressed in terms of the normal ordered correlations as follows:

$$\gamma_{ij}(\boldsymbol{r}, \boldsymbol{r}', t, t') = \frac{\langle \hat{E}_i^-(\boldsymbol{r}, t)\hat{E}_j^+(\boldsymbol{r}', t')\rangle}{(\langle \hat{E}_i^-(\boldsymbol{r}, t)\hat{E}_i^+(\boldsymbol{r}, t)\rangle\langle \hat{E}_j^-(\boldsymbol{r}', t')\hat{E}_j^+(\boldsymbol{r}', t')\rangle)^{1/2}}. \tag{1.1}$$

$\hat{E}_i(\boldsymbol{r}, t)$ denotes one component of the space- and time-dependent operator of the electric field. The $-$ and $+$ signs denote the negative- and positive-frequency parts of the operators (Glauber 1963); $\langle\ \rangle$ denotes the thermal ensemble average at temperature T. The modulus as well as the phase of γ_{ij} is directly related to the observed interference pattern created, for example, by a double-slit set-up. The modulus of γ measures the contrast, while the phase of γ specifies the maxima of the interference pattern (Mandel and Wolf 1965).

Recently, the temporal coherence properties of the blackbody radiation in restricted geometries were analysed and compared with those of radiation in isotropic infinite space (Steinle *et al* 1975, Baltes *et al* 1976, Eckhardt 1978a). In these papers the comparison was always made between volume-averaged quantities, and therefore only a global description of the temporal coherence was possible.

Here, the main interest is focused on the spatial dependence of the coherence in the slab resonator: temporal and spatial coherence will depend on the positions at which the field is considered.

2. Position-dependent temporal correlation functions

We consider the electromagnetic equilibrium fluctuations between two infinitely extended and perfectly conducting plates separated by a distance L. The x direction is chosen perpendicular to the plates so that the plates are described by the equations $x=0$ and $x=L$. The complete correlation tensors of the system in a representation which may be interpreted as an expansion around a two-dimensional radiation field and which is suited for numerical discussion were given in a preceding paper (Eckhardt 1978b, equations (6.12)–(6.39); hereinafter we will refer to this work as I).

Let $\boldsymbol{r}_2$ be the component of $\boldsymbol{r}$ in the yz plane, and $E_{ii}^{(N)}(\boldsymbol{r},\boldsymbol{r}',\tau)=\langle\hat{E}_i^-(\boldsymbol{r},\tau)\hat{E}_i^+(\boldsymbol{r}',0)\rangle$ and $H_{ii}^{(N)}(\boldsymbol{r},\boldsymbol{r}',\tau)=\langle\hat{H}_i^-(\boldsymbol{r},\tau)\hat{H}_i^+(\boldsymbol{r}',0)\rangle$ be the diagonal elements of the electric and magnetic correlation tensors respectively. Then we may write

$$E_{ii}^{(N)}(\boldsymbol{r},\boldsymbol{r}',\tau)=E_{ii}^{(N)}(|\boldsymbol{r}_2-\boldsymbol{r}_2'|,x,x',\tau).$$

In the following we put $\boldsymbol{r}_2=\boldsymbol{r}_2'$. Using the abbreviations

$$\alpha=\hbar\pi c/k_{\mathrm{B}}TL, \tag{2.1}$$

$$\kappa=2L^4/\pi^3c\hbar, \tag{2.2}$$

$$\mu=\tau k_{\mathrm{B}}T/\hbar \qquad \text{(thermodynamic reduced time)}, \tag{2.3}$$

$$\xi=\pi x/L, \tag{2.4}$$

$$\xi'=\pi x'/L, \tag{2.5}$$

we obtain from I

$$\kappa\alpha^3E_{xx}^{(N)}(x,x',\tau)$$

$$=4\Big(\zeta(3,1-\mathrm{i}\mu)+\sum_{p=1}^{\infty}\sum_{n=1}^{\infty}\sum_{j=2}^{3}\mathrm{e}^{-n\alpha(p-\mathrm{i}\mu)}\frac{(n\alpha)^{3-j}}{(p-\mathrm{i}\mu)^j}[2\cos n\xi\cos n\xi']\Big), \tag{2.6}$$

$$\kappa x^3E_{yy}^{(N)}(x,x',\tau)$$

$$=\kappa\alpha^3E_{zz}^{(N)}(x,x',\tau)$$

$$=2\sum_{p=1}^{\infty}\sum_{n=1}^{\infty}\sum_{j=1}^{3}\mathrm{e}^{-n\alpha(p-\mathrm{i}\mu)}\frac{(n\alpha)^{3-j}}{(p-\mathrm{i}\mu)^j}[2\sin n\xi\sin n\xi'], \tag{2.7}$$

$$\kappa\alpha^3H_{xx}^{(N)}(x,x',\tau)$$

$$=4\sum_{p=1}^{\infty}\sum_{n=1}^{\infty}\sum_{j=2}^{3}\mathrm{e}^{-n\alpha(p-\mathrm{i}\mu)}\frac{(n\alpha)^{3-j}}{(p-\mathrm{i}\mu)^j}[2\sin n\xi\sin n\xi'], \tag{2.8}$$

$$\kappa\alpha^3H_{yy}^{(N)}(x,x',\tau)$$

$$=\kappa\alpha^3H_{zz}^{(N)}(x,x',\tau)$$

$$=2\zeta(3,1-\mathrm{i}\mu)+2\sum_{p=1}^{\infty}\sum_{n=1}^{\infty}\sum_{j=1}^{3}\mathrm{e}^{-n\alpha(p-\mathrm{i}\mu)}\frac{(n\alpha)^{3-j}}{(p-\mathrm{i}\mu)^j}[2\cos n\xi\cos n\xi']. \tag{2.9}$$

In (2.6) and (2.9) ζ denotes the generalised Riemann zeta function which is defined by the series

$$\zeta(s,a)=\sum_{n=0}^{\infty}(n+1-a)^{-s}.$$

In the limit $\alpha \to \infty$ only the first terms in (2.6) and (2.9) are left. They represent the isotropic two-dimensional radiation field: the wavevectors of all excited modes lie in the yz plane.

Owing to the rapid convergence of the series in (2.6)–(2.9) these formulae are most suitable for numerical discussions. If we put $\xi = \xi'$ in (2.6)–(2.9) and perform the integration over x we obtain the known results (Eckhardt 1978a, equations (21)–(24)). The integration corresponds to the replacement of the square brackets in (2.6)–(2.9) by 1.

To make contact with the results of Baltes *et al* (1976) we will also calculate the x- and x'-dependent correlations in the $\alpha \to 0$ representation. To do this we will follow the procedure described in I (§ 6.2). We find

$$\kappa\alpha^4 E_{xx}^{(N)}(x, x', \tau) = \sum_{n=1}^{\infty} \sum_{p=-\infty}^{\infty} \sum_{i=1}^{4} [(n - i\mu)^2 + \psi_i^2]^{-2}, \tag{2.10}$$

$$\kappa\alpha^4 E_{yy}^{(N)}(x, x', \tau) = \sum_{n=1}^{\infty} \sum_{p=-\infty}^{\infty} \sum_{i=1}^{4} (-1)^i \frac{(n - i\mu)^2 - \psi_i^2}{[(n - i\mu)^2 + \psi_i^2]^3}, \tag{2.11}$$

$$\kappa\alpha^4 H_{xx}^{(N)}(x, x', \tau) = \sum_{n=1}^{\infty} \sum_{p=-\infty}^{\infty} \sum_{i=1}^{\infty} (-1)^i [(n - i\mu)^2 + \psi_i^2]^{-2}, \tag{2.12}$$

$$\kappa\alpha^4 H_{yy}^{(N)}(x, x', \tau) = \sum_{n=1}^{\infty} \sum_{p=-\infty}^{\infty} \sum_{i=1}^{4} \frac{(n - i\mu)^2 - \psi_i^2}{[(n - i\mu)^2 + \psi_i^2]^3}. \tag{2.13}$$

In (2.10)–(2.13) we have defined the quantities

$$\begin{aligned} \psi_1 &= (\xi + \xi' + 2\pi p)/\alpha, & \psi_2 &= (\xi - \xi' + 2\pi p)/\alpha, \\ \psi_3 &= (\xi + \xi' - 2\pi p)/\alpha, & \psi_4 &= (\xi' - \xi + 2\pi p)/\alpha. \end{aligned} \tag{2.14}$$

The $p = 0$ terms in (2.10)–(2.13) represent the well-known correlations in the half-space (Agarwal 1975, Fox-Keller 1965); $\kappa\alpha^4$ and ξ/α are independent of L (only thermodynamic reduced quantities are involved), there is only one reflection at $x = 0$ for the $i = 1, 3$ terms, and no reflection at all for the $i = 2, 4$ terms. $\pm p$ may be interpreted as the number of reflections at the wall $x = L$. A general mathematical concept of the multiple-reflection expansions used to calculate the density of states in finite systems was developed by Balian and Bloch (1970a, b, 1972); see also Balian and Duplantier (1977), Lukosz (1971) and Brown and Maclay (1969). If we put $x = x'$ and integrate over x the $p = 0$, $i = 2, 4$ terms yield $\zeta(4, 1 - i\mu)$, i.e. the correlation functions of the infinite isotropic space. Considering the relation

$$\sum_{p=-\infty}^{\infty} \int_{p}^{p+1} f(y)\, dy = \int_{-\infty}^{\infty} f(y)\, dy$$

in the terms $i = 1, 3$, and expressing the $i = 2, 4$ terms ($p \neq 0$) by generalised ζ functions, we obtain the results of Baltes *et al* (1976).

Owing to the relatively slow convergence of the series (2.10)–(2.13) the $\alpha \to 0$ representation is not suited for a discussion of the coherence properties for arbitrary values of α and μ.

If we add up the traces of the electric and magnetic correlation tensors ($x = x'$) the x dependence vanishes, i.e. the spectral and total energy density in the slab as well as in the half-space are r-independent (Eckhardt 1978a, b).

3. Position-dependent temporal coherence

In this section we restrict ourselves to the discussion of the spatially dependent coherence properties of the electric autocorrelation functions. Analogous considerations can be made for the magnetic fields. The temporal x-dependent coherence properties are determined by the modulus $|\gamma_{ii}(x, \tau)|$ and the phase $\phi_{ii}(x, \tau) = \tan^{-1}(\mathrm{Im}\, E_{ii}^{(N)}(x, \tau)/\mathrm{Re}\, E_{ii}^{(N)}(x, \tau))$ of the complex degree of coherence. Splitting up the correlations (2.6)–(2.9) into real and imaginary parts we can perform the summation over n (Eckhardt 1978a, b). The resultant formulae are basic for our numerical discussions.

For large $\alpha (\alpha \geqslant 8)$, γ_{xx} shows the coherence properties of a two-dimensional radiation field, while γ_{yy} reveals a damped one-mode behaviour. In this regime both radiation fields are independent of x, and therefore we find no differences compared with the volume-averaged quantities.

With decreasing α, modes which have non-vanishing x components of the wavevector ($k_x = n\pi/L = 1, 2, 3, \ldots$) successively contribute to γ_{xx}. In γ_{yy}, damped eigenmodes with $k_x = n\pi/L$, $n \geqslant 2$ become important. Consequently, both radiation fields are x-dependent.

In figures 1 and 2 we have plotted the modulus of γ_{yy} as a function of μ for different values of x, for $\alpha = 4$ and $\alpha = 2$ respectively. With the exception of $\mu\alpha \simeq 2\pi n$ the curves for $x/L < \frac{1}{3}$ lie below and the curves for $x/L > \frac{1}{3}$ lie above the averaged curve. The $x/L = \frac{1}{3}$ curve is nearly identical with the averaged one. The lowest ($x/L = 0$) and highest ($x/L = \frac{1}{2}$) curves are displayed in the figures. We note that the x dependence nearly disappears for $\mu\alpha \simeq 2\pi n$ (this is more true for $\alpha = 4$ than for $\alpha = 2$) and is strongly marked between these values.

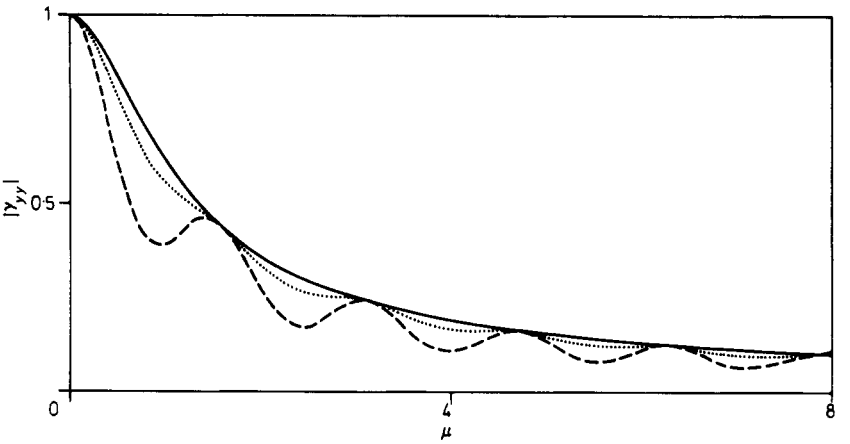

Figure 1. Modulus of the temporal coherence function for the infinite slab resonator, component parallel to the plates, $|\gamma_{yy}|$ for $\alpha = 4$, i.e. $LT = 0{\cdot}18$ cm K, against the thermodynamic reduced time $\mu = \tau k_B T/\hbar$ for $x = 0$ (broken curve) and $x = L/2$ (full curve). The volume-averaged case (dotted curve) is shown for comparison.

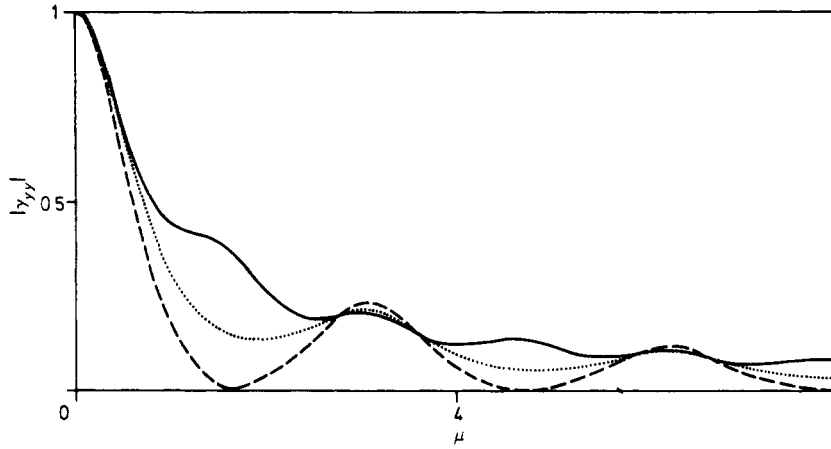

Figure 2. As in figure 1 with $\alpha = 2$, i.e. $LT = 0{\cdot}36$ cm K.

For $\alpha = 4$ the phase of γ_{yy} is nearly independent of x. In figure 3 we see that for $\alpha = 2$ and for different values of x the phase of γ_{yy} oscillates around the averaged curve. The limit curves are also given by $x/L = 0$ and $x/L = \frac{1}{2}$, and the $x/L = \frac{1}{3}$ curve is indistinguishable from the averaged curve. For $\alpha\mu \simeq \pi n$ the x dependence disappears.

These characteristic features can be extracted from the $\alpha \to \infty$ representation if in γ_{yy} all terms proportional to $e^{-n\alpha}$ are neglected for $n \geq 2$ (i.e. in (2.7) only the terms $n = 1$,

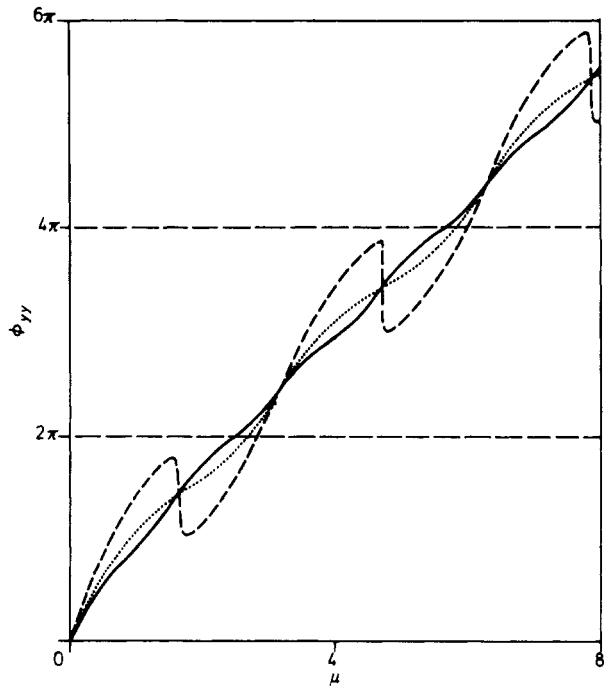

Figure 3. Phase angle $\phi_{yy} = \arg \gamma_{yy}$ of the temporal coherence function parallel to the plates for $\alpha = 2$ as a function of $\mu = \tau k_B T/\hbar$ for $x = 0$ (broken curve) and $x = L/2$ (full curve). The volume-averaged case (dotted curve) is shown for comparison.

$p = 1, n = 2, p = 1$ and $n = 1, p = 2$ are taken into consideration). In this approximation we obtain

$$|\gamma_{yy}| = (1+\mu^2)^{-1/2}\left[1+e^{-\alpha}\left(4(\cos\mu\alpha - 1)4\cos^2\xi + \frac{\mu^2}{2(4+\mu^2)}\right)\right], \tag{3.1}$$

$$\tan\phi_{yy} = \frac{\sin\mu\alpha + \mu\cos\mu\alpha}{\cos\mu\alpha - \mu\sin\mu\alpha}\left\{1+e^{-\alpha}\left[\left(4\sin\mu\alpha 4\cos^2\xi - \frac{\mu}{4+\mu^2}\right)\right.\right.$$
$$\left.\left.\times\left(\frac{1-\mu^2}{1+\mu^2}\frac{1}{2}\sin 2\mu\alpha + \frac{\mu}{1+\mu^2}\cos 2\mu\alpha\right)^{-1}\right]\right\}. \tag{3.2}$$

Replacing $4\cos^2\xi$ by 1 in (3.1) and (3.2) we obtain the corresponding expressions for the volume-averaged quantities $|\gamma_{yy}|$ and ϕ_{yy}, and if $4\cos^2\xi = 1$, i.e. $x = L/3$, these expressions are equal. The factor in front of $\cos^2\xi$ vanishes in (3.1) if $\alpha\mu = 2\pi n$ and in (3.2) if $\alpha\mu = \pi n$. Between these nodes, which represent the local maxima ($\cos\alpha\mu - 1 = 0$), the curve is modulated by the factor $4\cos^2\xi$ compared with the averaged behaviour.

Therefore equations (3.1) and (3.2) describe the coherence properties well for $\alpha = 4$. Terms proportional to $1/\alpha$ compared with 1 were neglected and hence the description (3.1) and (3.2) cannot be as good for $\alpha = 2$.

In figures 4 and 5 we have plotted the modulus and phase of γ_{yy} for $\alpha = 0{\cdot}5$. In the higher-temperature regime ($\alpha = 0{\cdot}5 \Rightarrow LT = 1{\cdot}44$ cm K) many terms in (2.7) have to be considered, and the two-mode approximation is totally unsuitable.

For small $\alpha (\alpha < 1)$ maxima are found in $|\gamma_{yy}|$ for $\alpha\mu = 2\pi p$, i.e. for $\tau c = 2Lp$, $p = 1, 2, 3, \ldots$ (Baltes *et al* 1976, Eckhardt 1978a).

In addition there are maxima in $|\gamma_{yy}|$ for arbitrary values of x if $\tau c = 2(x \pm Lp)$, $p = 0, 1, 2, \ldots$, i.e. maxima are found for time differences τ necessary to form closed trajectories with respect to the point x after p reflections at the wall $x = L$. (The maximum in figure 4 corresponds to $c\tau = 2x$.) Owing to the damping the maxima disappear with increasing p.

With the exception of these additional maxima the volume-averaged curves are identical with the x-dependent ones if x/L is not too small.

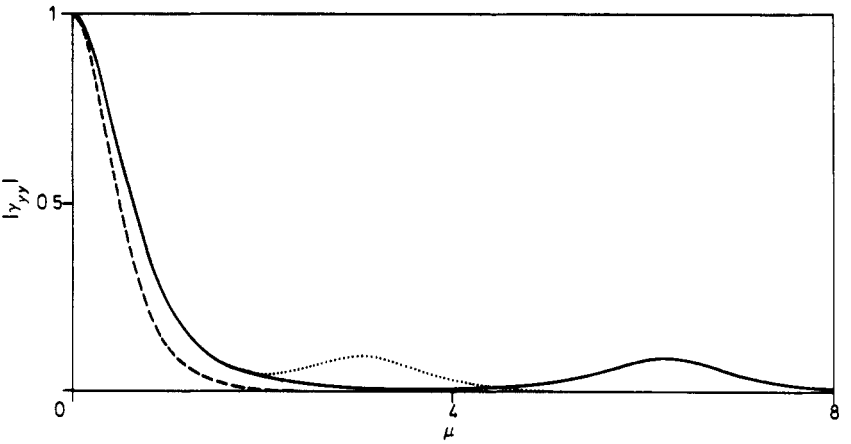

Figure 4. Modulus of the temporal coherence function for the infinite slab resonator, component parallel to the plates, $|\gamma_{yy}|$ for $\alpha = 0{\cdot}5$, i.e. $LT = 0{\cdot}72$ cm K, as a function of $\mu = \tau k_B T/\hbar$ for $x = 0$ (broken curve), $x = L/4$ (dotted curve) and $x = L/2$ (full curve).

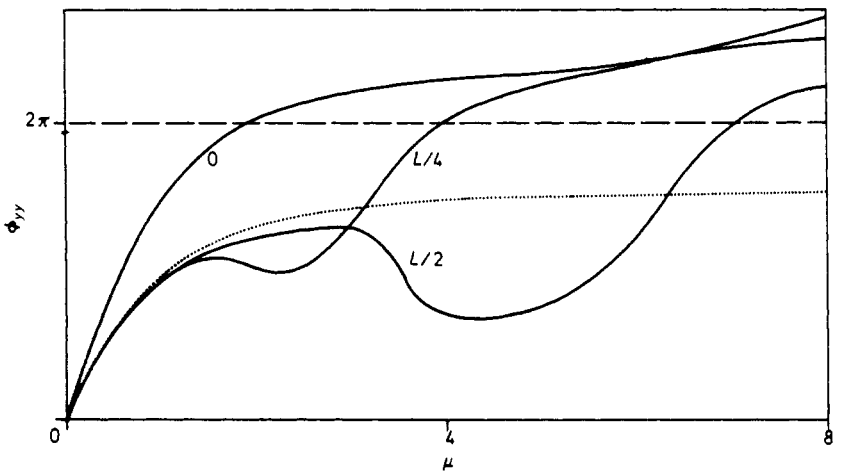

Figure 5. Phase angle $\phi_{yy} = \arg \gamma_{yy}$ of the temporal coherence function parallel to the plates for $\alpha = 0{\cdot}5$ as a function of $\mu = \tau k_B T/\hbar$ for $x = 0$, $L/4$ and $L/2$. The volume-averaged case (dotted curve) is shown for comparison.

In figure 5 we see that the phases show complete cycles even for $\tau c < 2L$: there are already closed trajectories for $\tau c = 2x$.

Considering equation (2.11) we can understand these characteristic features qualitatively. The denominator of the real and imaginary part of (2.11) will be minimal if $\mu = \psi_i$, i.e. after the time necessary to return from x to x' after $\pm p$ reflections at $x = L$. For $x = x'$ the above interpretation applies.

In the $\alpha \gg 1$ approximation for γ_{xx} we take into account two parts: the two-dimensional radiation field, and the lowest mode with non-vanishing component of the wavevector perpendicular to the plates. We find

$$|\gamma_{xx}| = \frac{|\zeta(3, 1-i\mu)|}{\zeta(3)}\Big\{1 + |\zeta(3, 1-i\mu)|^{-2} \times\Big[\Big(\frac{1-\mu^2}{(1+\mu^2)^2}\operatorname{Re}\zeta(3, 1-i\mu) + \frac{2\mu}{(1+\mu^2)^2}\operatorname{Im}\zeta(3, 1-i\mu)\Big)\cos\mu\alpha + \Big(\frac{1-\mu^2}{(1+\mu^2)^2}\operatorname{Im}\zeta(3, 1-i\mu) - \frac{2\mu}{(1+\mu^2)^2}\operatorname{Re}\zeta(3, 1-i\mu)\Big)\sin\mu\alpha - \frac{|\zeta(3, 1-i\mu)|^2}{\zeta(3)}\Big]\alpha\, e^{-\alpha}\, 2\cos^2\xi\Big\}, \tag{3.3}$$

$$\tan\phi_{xx} = \frac{\operatorname{Im}\zeta(3, 1-i\mu)}{\operatorname{Re}\zeta(3, 1-i\mu)}\Big\{1 + (1+\mu^2)^{-2} \times\Big[\Big(\frac{2\mu}{\operatorname{Im}\zeta(3, 1-i\mu)} - \frac{1-\mu^2}{\operatorname{Re}\zeta(3, 1-i\mu)}\Big)\cos\mu\alpha + \Big(\frac{1-\mu^2}{\operatorname{Im}\zeta(3, 1-i\mu)} + \frac{2\mu}{\operatorname{Re}\zeta(3, 1-i\mu)}\Big)\sin\mu\alpha\Big]2\cos^2\zeta\alpha\, e^{-\alpha}\Big\}. \tag{3.4}$$

Replacing $2\cos^2\xi$ by 1 in (3.3) and (3.4) we obtain the corresponding expressions of the averaged quantities, and for $x = L/4$ both approximations are equal.

If $\alpha\mu = 2\pi n$ in (3.3) and if $n = \pi n$ in (3.4), the factor in front of $\alpha\, e^{-\alpha}\, 2\cos^2\xi$ becomes so small that the x dependence nearly vanishes. Between these values the curves for $x < L/4$ lie below and the curves for $x > L/4$ lie above the averaged ones. We find the same qualitative deviations from the averaged properties as we found for γ_{yy}. Furthermore we may conclude from (2.10) that the qualitative features of γ_{yy} in the $\alpha < 1$ regime are also valid for γ_{xx}. We have not shown the γ_{xx} curves as the graphs are less instructive owing to the stronger damping in γ_{xx}.

4. Spatial correlation functions

To complete the description of the electromagnetic fluctuations in the slab, we study the spatial coherence ($\tau = 0$). We restrict ourselves to the discussion of the diagonal elements of the electric correlation tensor which determines the optical properties. We define the temperature-scaled distance vector in the yz plane

$$\boldsymbol{R} = (R_y, R_z) = (k_B T/\hbar c)(y - y', z - z'), \qquad |\boldsymbol{R}| = R, \tag{4.1}$$

the length-scaled quantities

$$\phi_1 = \pi(x/L - x'/L), \tag{4.2}$$

$$\phi_2 = \pi(x/L + x'/L), \tag{4.3}$$

and

$$\sigma = (p^2 + R^2)^{1/2}. \tag{4.4}$$

We obtain the formulae (cf I, equation (6.12))

$$\begin{aligned}\kappa\alpha^3 E_{xx}^{(N)}(\boldsymbol{r}, \boldsymbol{r}', t = t') &= \sum_{p=1}^{\infty} \frac{2p^2 - R^2}{\sigma^5} + \sum_{p=1}^{\infty} [-\alpha^2\sigma^{-3}R^2(Q_3(\alpha\sigma, \phi_1) + Q_3(\alpha\sigma, \phi_2)) \\ &\quad + \alpha\sigma^{-4}(2p^2 - R^2)(Q_2(\alpha\sigma, \phi_1) + Q_2(\alpha\sigma, \phi_2)) \\ &\quad + \sigma^{-5}(2p^2 - R^2)(Q_1(\alpha\sigma, \phi_1) + Q_1(\alpha\sigma, \phi_2))],\end{aligned} \tag{4.5}$$

$$\begin{aligned}\kappa\alpha^3 E_{yy}^{(N)}(\boldsymbol{r}, \boldsymbol{r}', t = t') &= \sum_{p=1}^{\infty} [\alpha^2\sigma^{-3}(p^2 + R_y^2)(Q_3(\alpha\sigma, \phi_1) - Q_3(\alpha\sigma, \phi_2)) \\ &\quad + \alpha\sigma^{-4}(p^2 + R_y^2 - 2R_z^2)(Q_2(\alpha\sigma, \phi_1) - Q_2(\alpha\sigma, \phi_2)) \\ &\quad + \sigma^{-5}(p^2 + R_y^2 - 2R_z^2)(Q_1(\alpha\sigma, \phi_1) - Q_1(\alpha\sigma, \phi_2))].\end{aligned} \tag{4.6}$$

In (4.5) and (4.6) we have defined the functions

$$Q_l(\alpha\sigma, \phi) = \sum_{n=1}^{\infty} (-1)^{l-1} \frac{\partial^{l-1}}{\partial(\alpha\sigma)^{l-1}} e^{-\alpha\sigma n} \cos\phi n, \qquad l = 1, 2, 3, \tag{4.7}$$

which can be expressed in closed form (see equations (6.2)–(6.4) in I). We note that $E_{xx}^{(N)}$ depends only on the modulus of $\boldsymbol{R}$, while in $E_{yy}^{(N)} R_y$ and R_z are involved.

Equations (4.5) and (4.6) may be interpreted as the $\alpha \to \infty$ representation of the correlation functions (expansion around the two-dimensional radiation field, Eckhardt 1978b). We have not reported the $\alpha \to 0$ representation because it is not suitable for quantitative discussion (see e.g. equation (6.40) in I with $\mu = 0$).

5. Longitudinal and lateral coherence

In analogy to the work of Bourett (1960) we will discuss the special forms of spatial coherence which are designated as longitudinal and lateral correlations. Owing to the vector character of the fields the coherence properties can be described more easily if we restrict ourselves to these two special cases. For longitudinal and lateral correlations the spatial distance is respectively parallel and perpendicular to the direction of the autocorrelated field component.

In the infinite-space limit all autocorrelated field components are equal, and therefore only one longitudinal and one lateral correlation have to be studied. In our case, however, we may study five different functions: (i) $\gamma_{xx}^{\text{long}}(R=0; x, x')$; (ii) $\gamma_{xx}^{\text{lat}}(R; x=x')$; (iii) $\gamma_{yy}^{\text{long}}(R_y, R_z=0; x=x')$; (iv) $\gamma_{yy}^{\text{lat 1}}(R_y=0, R_z; x=x')$; (v) $\gamma_{yy}^{\text{lat 2}}(R_y=R_z=0; x=x')$. In infinite space the longitudinal and lateral coherence functions depend only on the temperature-scaled distance of the considered space points. There is no explicit temperature dependence (Bourett 1960).

In figure 6 we have plotted $\gamma_{xx}^{\text{long}}$ for different values of α. $x-x'$ was chosen symmetrical to the plane $x=L/2$ (i.e. $x+x'=L$). If we display $\gamma_{xx}^{\text{long}}$ against the temperature-scaled distance $(k_B T/\hbar c)\,(x-x')$ for $\alpha < 0{\cdot}5$ the isotropic space limit is approached. On the other hand for $\alpha \gg 1$ $\gamma_{xx}^{\text{long}}$ is independent of x:

$$\gamma_{xx} \to \frac{1}{2\zeta(3)} \sum_{p=1}^{\infty} \frac{2p^2 - R^2}{(p^2+R^2)^{5/2}}. \tag{5.1}$$

For fixed $x-x'$ the x dependence of $\gamma_{xx}^{\text{long}}$ can be studied. We find that the coherence is slightly increased compared with the symmetric case if x (or x') is close to the boundary.

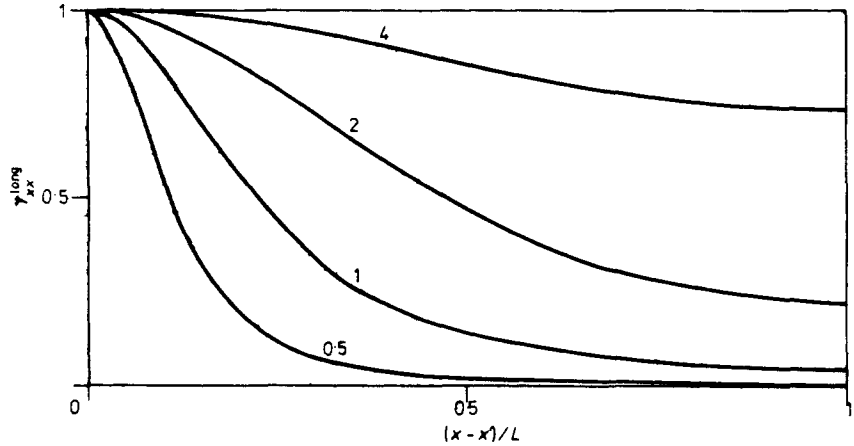

Figure 6. Spatial coherence function for the infinite slab resonator, component perpendicular to the plates, $\gamma_{xx}^{\text{long}}$ against the length-scaled distance $(x-x')/L$ for $\alpha = 0{\cdot}5, 1, 2, 4$, i.e. $LT = 1{\cdot}44, 0{\cdot}72, 0{\cdot}36, 0{\cdot}18$ cm K and $x+x' = L$.

This is also valid for $\alpha < 0{\cdot}5$, i.e. for very small α the influence of the boundaries is noticeable (see also figures 1 and 2 in I).

In figure 7 γ_{xx}^{lat} is displayed as a function of the temperature-scaled distance in the yz plane for $x = x' = L/2$. For $\alpha \leqslant 0{\cdot}5$ the infinite-isotropic-space limit is reached. For $\alpha \to \infty$ the coherence function is given by (5.1) (isotropic two-dimensional radiation field).

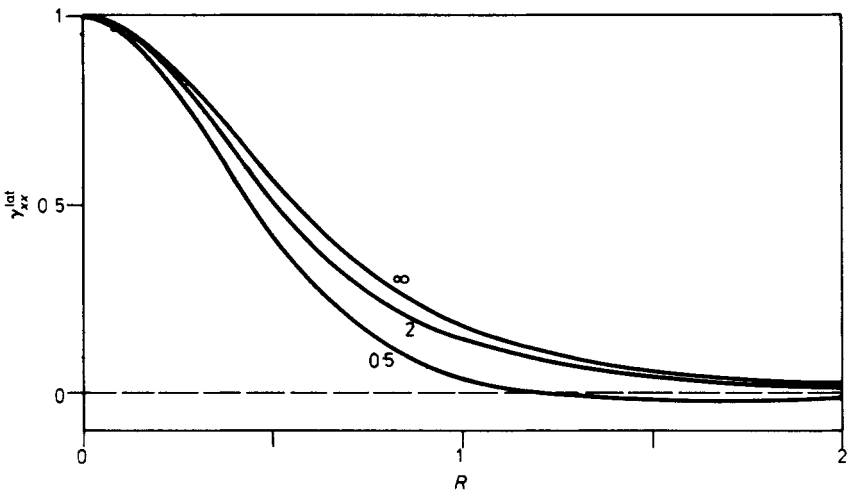

Figure 7. Spatial coherence function for the infinite slab resonator, component perpendicular to the plates, γ_{xx}^{lat} as a function of the thermodynamic reduced distance $R = (k_B T/\hbar c)[(y-y')^2 + (z-z')^2]^{1/2}$ for $\alpha = 0{\cdot}5, 2, \infty$ and $x = x' = L/2$.

In figure 8 we have plotted a characteristic cut through figure 7 which reveals the x dependence of γ_{xx}^{lat}. Near the boundary there are deviations from the isotropic limit even for $\alpha \leqslant 0{\cdot}5$. With increasing α the x dependence decreases. The isotropic space limit in the $\alpha \leqslant 0{\cdot}5$ regime is approached more closely as x and x' move away from the boundaries. For $\gamma_{yy}^{\text{long}}$ the same property is shown in figures 9 and 10. In contrast to $\gamma_{xx}^{\text{long}}$ the coherence decreases with increasing α and fixed R_y:

$$\gamma_{yy} \to \frac{1+R_y^2}{(1+R^2)^{3/2}} \exp[-\alpha[(1+R^2)^{1/2}-1]]. \tag{5.2}$$

For $\alpha \leqslant 0{\cdot}5$ the lateral coherence functions of γ_{yy} approach the isotropic space limit. Studying the x dependence of $\gamma_{yy}^{\text{lat}\,1}$ we find a behaviour similar to that for $\gamma_{yy}^{\text{long}}$: the coherence increases with increasing distance to the boundary $x = 0$. The x dependence of $\gamma_{yy}^{\text{lat}\,2}$ shows the same characteristic features as the x dependence of $\gamma_{xx}^{\text{long}}$.

6. Conclusions

In this paper we have discussed the space dependence of the coherence of blackbody radiation between two infinitely extended, parallel metallic plates. In contrast with infinite isotropic space, closed classical trajectories are possible in this system and these lead to finite Poincaré recurrence times.

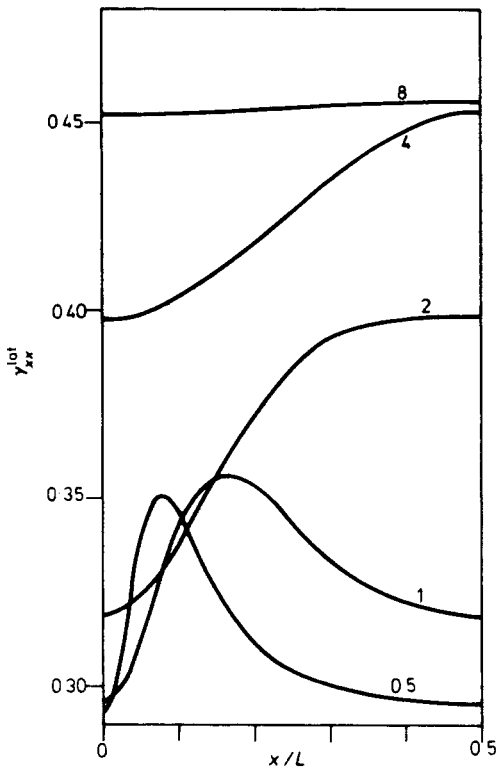

Figure 8. Spatial coherence function for the infinite slab resonator, component perpendicular to the plates, γ_{xx}^{lat} against the position x/L between the plates for $\alpha = 0{\cdot}5$, 1, 2, 4, 8 and $R = 0{\cdot}6$.

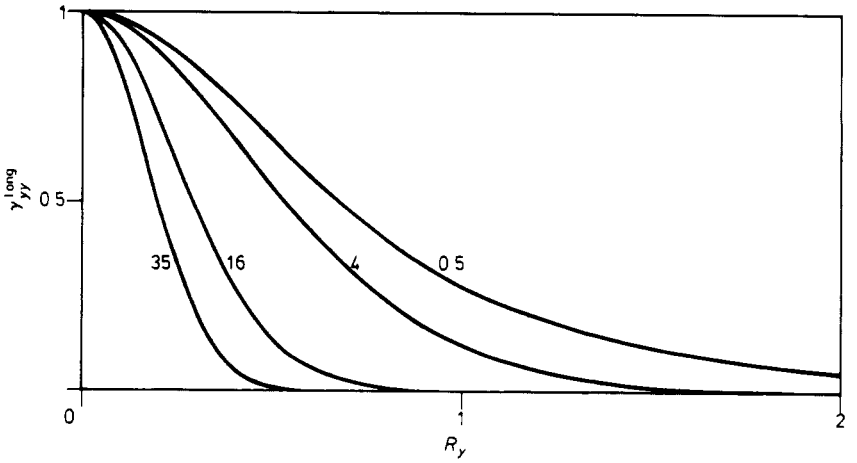

Figure 9. Spatial coherence function for the infinite slab resonator, component parallel to the plates, γ_{yy}^{long} against $R_y = (k_B T/\hbar c)|y - y'|$ for $\alpha = 0{\cdot}5$, 4, 16, 35 and $x = x' = L/2$.

For $\alpha < 1$ the x dependence shows additional peaks in the modulus of the degree of temporal coherence at $\tau = 1/c(x \pm x' \pm 2pL)$. Classical trajectories which start from a point x between the plates return after p reflections to this point. For $\alpha \gg 1$ the

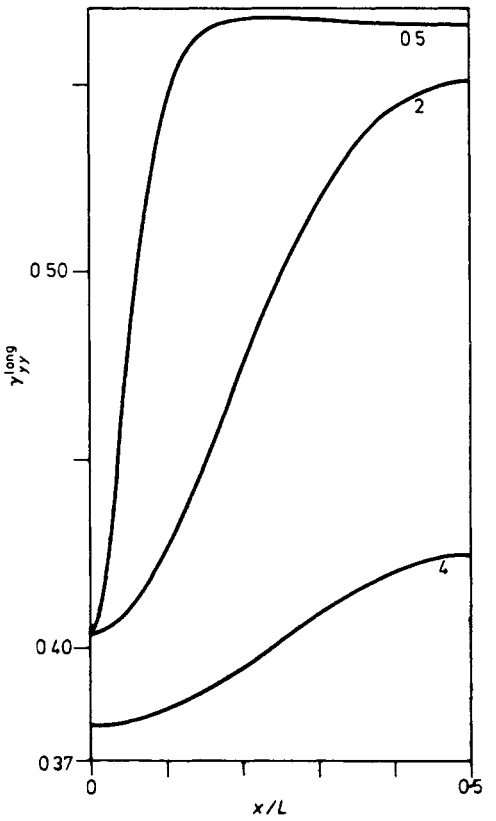

Figure 10. Spatial coherence function for the infinite slab resonator, component parallel to the plates, γ_{yy}^{long} as a function of the position x/L between the plates for $\alpha = 0{\cdot}5, 2, 4$ and $R_y = 0{\cdot}6$.

temporal coherence properties are determined by the superposition of two damped modes (γ_{yy}) and the superposition of a two-dimensional radiation field with one discrete and damped mode (γ_{xx}). With increasing time the damping leads to the disappearance of the peaks in the modulus of γ. The damping is due to the continuous part of the spectrum.

The lateral and longitudinal degrees of spatial coherence ($\tau = 0$) approach the infinite-space limit for $\alpha \leqslant 0{\cdot}5$ (LT $> 1{\cdot}44$) if x and x' are lying symmetrically to the plane $x = L/2$ or if $x = x' = L/2$. For large α, γ_{xx} is independent of x and x' and describes the coherence properties of an isotropic two-dimensional radiation field, while γ_{yy} may be considered as the coherence function of a damped single mode with wavevector $\boldsymbol{k}' = (\pi/L, 0, 0)$.

References

Agarwal G S 1975 *Phys. Rev.* A **11** 230–42
Balian R and Bloch C 1970a *Ann. Phys.* **60** 401–47
—— 1970b *Ann. Phys.* **64** 271–307
—— 1972 *Ann. Phys.* **69** 76–160

Balian R and Duplantier B 1977 *Ann. Phys.* **104** 300–35
Baltes H P, Steinle B and Pabst M 1976 *Phys. Rev.* A **13** 1866–73
Bourett R C 1960 *Nuovo Cim.* **18** 347–56
Brown L S and Maclay G J 1969 *Phys. Rev.* **184** 1272–9
Eckhardt W 1978a *Phys. Rev.* A **17** 1093–9
—— 1978b *Z. Phys.* B **31** 217–31
Fox-Keller E 1965 *Phys. Rev.* B **139** 202–11
Glauber R J 1963 *Phys. Rev.* **130** 2529–39
Lukosz W 1971 *Z. Phys.* **258** 99–107
—— 1973 *Z. Phys.* **262** 327–48
Mandel L and Wolf E 1965 *Rev. Mod. Phys.* **37** 231–87
Mehta C L and Wolf E 1964a *Phys. Rev.* A **134** 1143–9
—— 1964b *Phys. Rev.* A **134** 1149–53
—— 1967 *Phys. Rev.* **161** 1328–34
Sarfatt J 1963 *Nuovo Cim.* **28** 1119–29
Steinle B, Baltes H P and Pabst M 1975 *Phys. Rev.* A **12** 1519–24